The Actin-Binding Interface of a Myosin III Is Phosphorylated *in Vivo* in Response to Signals from a Circadian Clock†

Helene L. Cardasis,[‡,§,||] Stanley M. Stevens Jr.,[§,⊥] Scott McClung,[§] Karen E. Kempler,[#] David H. Powell,[‡] John R. Eyler,[‡] and Barbara-Anne Battelle*[,#]

Department of Chemistry, University of Florida, Gainesville, Florida 32611, Proteomics Core, ICBR, University of Florida, Gainesville, Florida 32611, and The Whitney Laboratory for Marine Bioscience and the Department of Neuroscience, University of Florida, St. Augustine, Florida 32080

Received July 17, 2007; Revised Manuscript Received September 25, 2007

ABSTRACT: Class III unconventional myosins are critical for the normal function of auditory hair cells and the function and maintenance of photoreceptors; however, the roles of class III myosins in these sensory cells are unknown. Class III myosins are unique in that they have a kinase domain at their N-terminus; thus, they may have both signaling and motor functions. In the horseshoe crab *Limulus polyphemus*, enhanced phosphorylation of an abundant, photoreceptor specific class III myosin at night correlates with well-characterized circadian changes in photoreceptor structure and function. Thus, the *Limulus* visual system may be particularly useful for investigating the properties, modulation, and functions of a class III myosin. Previously, we showed that two sites within the actin interface of full-length *Limulus* myosin III expressed in baculovirus are substrates for both cyclic AMP-dependent protein kinase and autophosphorylation. In the current study, mass spectrometry was used to show that these same sites are phosphorylated in the endogenous protein extracted from *Limulus* lateral eye, and that enhanced phosphorylation at these sites occurs *in vivo* in response to natural circadian clock input to these eyes. These findings demonstrate *in vivo* changes in myosin III phosphorylation in response to a natural stimulus. This phosphorylation may modulate myosin III−actin interactions.

Class III unconventional myosins are present in the photoreceptors of invertebrates and vertebrates including humans (*1*−*8*) and in the auditory hair cells of mice and humans (*9*, *10*). In *Drosophila* photoreceptors, class III myosins have been implicated in diverse processes impacting the photoresponse (*11*−*15*), and the loss of class III myosins leads to photoreceptor degeneration (*1*, *11*). In humans, a mutation in one of two class III myosin genes leads to progressive hearing loss (*9*). Thus, class III myosins are critical for the normal function of photoreceptors and auditory hair cells and, in the case of *Drosophila*, for the survival of photoreceptors.

Class III myosins may express both signaling and motor functions because in addition to the myosin motor, neck, and tail domains typically found in other unconventional myosins, they have a kinase domain at their N-terminus. All class III myosins examined so far are active kinases capable of phosphorylating their own myosin motor domain and other substrates (*16*−*19*); however, motor activity has not been observed in all of these proteins. Human myosin IIIA (HMYO3A[1]) is a motor (*17*, *18*, *20*), but motor activity for *Drosophila* myosin III (NINAC) has not been demonstrated, and there is good evidence that *Limulus* myosin III (LpMYO3) is not a motor (*19*).

LpMYO3, the focus of this study, is abundant in photoreceptors (see Results) and concentrates over the actin-rich photosensitive microvilli during the day under conditions of natural illumination (*2*, *21*). It was first identified as a photoreceptor-specific phosphoprotein that becomes more heavily phosphorylated at night in response to signals from a central circadian clock. Circadian signals reach *Limulus* eyes via well-characterized efferent neurons that project to the eyes through the optic nerves (*22*). These neurons utilize the biogenic amine octopamine (OA) as their transmitter (*23*−*25*), and the application of OA to *Limulus* eyes elevates

† Supported by NSF Grants (IBN and IOB) to B.-A.B and the University of Florida's ICBR Proteomics Core Facility.

* Corresponding author. Mailing address: Whitney Laboratory for Marine Bioscience, University of Florida, 9505 Ocean Shore Blvd., St. Augustine, FL 32080. Tel: 904-461-4022. Fax: 904-461-4008. E-mail: Battelle@whitney.ufl.edu.

‡ Department of Chemistry.

§ Proteomics Core of the ICBR.

Whitney Laboratory for Marine Bioscience and the Department of Neuroscience.

|| Current address: Skirball Institute of Biomolecular Medicine, New York University, New York, NY 10016. E-mail: helene.cardasis@med.nyu.edu.

⊥ Current address: Advanced Mass Spectrometry Laboratory, University of North Texas Health Science Center, 3500 Camp Bowie Blvd, Fort Worth, TX 76107. E-mail: sstevens@hsc.unt.edu.

[1] Abbreviations: ABC, ammonium bicarbonate; ACN, acetonitrile; a.i., absolute intensity; BSA, bovine serum albumin; DTT, dithiothreitol; EIC, extracted ion chromatogram; ESI, electrospray ionization; HAc, acetic acid; HMYO3A, human myosin IIIA; HPLC, high performance liquid chromatography; i.d., inner diameter; LC, liquid chromatography; LE, lateral eye; LON, lateral optic nerve; LpMYO3, *Limulus polyphemus* myosin III; MALDI, matrix-assisted laser desorption ionization; MeOH, methanol; MS, mass spectrometry; MS/MS, tandem mass spectrometry; m/z, mass-to-charge ratio; OA, octopamine; ONS, optic nerve section; PKA, cyclic AMP dependent kinase; PKC, protein kinase C; qTOF, quadrupole time-of-flight; SDS-PAGE, sodium dodecyl sulfate polyacrylamide gel electrophoresis; SIM, single ion monitoring.

10.1021/bi701409f CCC: $37.00
Published on Web 11/09/2007

the intracellular concentration of cAMP in photoreceptors (*26*) and activates cAMP-dependent protein kinase (PKA). LpMYO3 is a major substrate for this clock-driven activation of PKA (*2*, *27*−*29*).

Enhanced phosphorylation of LpMYO3 at night correlates with changes in the structure, electrophysiological properties, and gene expression of *Limulus* photoreceptors, changes thought to contribute to the enhanced sensitivity and responsiveness of the eyes to light at night (*29*−*32*). Clock input to the lateral eye (LE) during the night is also required to prime the LE to respond normally to light the next day. For example, the synchronous internalization, or shedding, of photosensitive membrane that normally occurs in LE photoreceptors at dawn happens only after the LE receives at least 3 h of nighttime clock input (*33*, *34*). Transient shedding can also be primed by treating LEs with OA or other drugs that elevate cAMP or activate PKA in photoreceptors (*35*, *36*). In addition, clock input during the night is required for normal light-driven pigment migration in photoreceptors during the day (*37*).

LpMYO3 phosphorylation may be involved in one or more of these clock-driven or clock-primed changes in photoreceptors. To understand the importance of LpMYO3 and its phosphorylation for photoreceptor function we must first understand the functions of the protein itself and the impact of phosphorylation on these functions.

We recently demonstrated that LpMYO3 expressed in baculovirus binds to actin with similar affinity in the presence and absence of ATP, and that it lacks actin-activated ATPase activity, a requirement for motor function (*19*). Furthermore, the predicted amino acid sequence of LpMYO3 shows that it lacks a salt bridge in its myosin motor-like domain (hereafter referred to as the myosin domain) that in other myosins is critical for ATP hydrolysis (*2*, *38*). These observations indicate that LpMYO3 is an actin binding protein but not a motor. We showed that LpMYO3 is an active kinase that has substrate specificities and pharmacological properties similar to PKA (*19*). Finally, we demonstrated that the same sites within the loop 2 actin binding interface of the myosin domain of expressed LpMYO3 are substrates for both PKA and intermolecular autophosphorylation (*19*). To our knowledge, this was the first demonstration of the phosphorylation of any myosin within the loop 2 actin-binding interface. The region of LpMYO3 that we identify as loop 2 was predicted by aligning the primary sequence of the myosin domain of LpMYO3 with that of other myosins.

Others have shown that the net charge of loop 2 is an important determinant of actin binding affinity (*39*, *40*). Phosphorylation of sites within loop 2 would clearly alter the net charge of this actin-binding interface; thus, the phosphorylation of sites within and near loop 2 of LpMYO3 may regulate its affinity for actin.

Most of our previous identifications of LpMYO3 phosphorylation sites were conducted with protein expressed in baculovirus. The two goals of the current study were to determine whether the sites phosphorylated in the baculovirus expressed protein are also phosphorylated in the endogenous protein and to determine which of the phosphorylation sites are regulated by circadian clock input *in vivo*. To achieve these goals, mass spectrometry (MS)-based methodologies for relative quantification were utilized. We examined dynamic changes in phosphorylation by applying a differential labeling technique developed by Ficarro et al. (*41*) and a label-free technique similar to that described by Bondarenko et al. (*42*) in conjunction with high performance liquid chromatography (HPLC)-electrospray ionization (ESI)-tandem mass spectrometry (MS/MS). From this MS-based analysis we determined that the phosphorylated sites identified in baculovirus expressed LpMYO3 are indeed phosphorylated in native LpMYO3 extracted from the LE and lateral optic nerve (LON). We also found that natural clock input enhances the level of phosphorylation of two of the previously identified PKA sites, S^{796} and S^{846}, but that the level of phosphorylation of S^{841}, a putative protein kinase C site within loop 2, is unchanged by clock input. These findings provide direct evidence for the enhanced phosphorylation of sites within the loop 2 actin binding interface of LpMYO3 in response to a natural stimulus *in vivo*.

EXPERIMENTAL PROCEDURES

Animals and Standard Reagents. Adult *Limulus* collected from the Indian River near Melbourne, FL, were maintained at the Whitney Laboratory in continuously flowing, natural seawater held between 18 °C and 20 °C. These animals were kept under diurnal illumination provided through a skylight in the aquarium room. Unless otherwise specified, reagents were obtained from either Fisher Scientific (Pittsburgh, PA) or Sigma-Aldrich (St. Louis, MO).

Quantification of LpMYO3 in Lateral Eye and Lateral Optic Nerve Extracts. Tissues were homogenized as described previously (*43*) and centrifuged for 20 min at room temperature at high speed (100 000*g*) (Airfuge, Beckman Instruments) to obtain a soluble cell fraction. An aliquot was denatured by sonication in sodium dodecyl sulfate (SDS) sample buffer (*44*). A separate aliquot was mixed with an equal volume of 2 M NaOH and heated at 60 °C to solubilize protein. The SDS-solubilized samples were fractionated by SDS polyacrylamide gel electrophoresis (SDS PAGE) on 7.5% acrylamide gels, and the gels were stained to visualize total protein with Coomassie Blue R-250. Scanned images of the dried, destained gels were digitized. The amount of LpMYO3 in the sample loaded was determined from the intensity of its Coomassie Blue-stained band relative to that of β-galactosidase standards processed on the same gel. Protein staining was quantified using Image Quant software (Amersham Biosciences). Total protein was determined using the Lowry method (*45*) from the NaOH solubilized samples with bovine serum albumin (BSA) as the standard.

Lateral Optic Nerve Transection, Lateral Eye and Lateral Optic Nerve Extraction, and Gel Purification of LpMYO3. At least one week before collecting the tissue used in assays of clock-driven changes in LpMYO3 phosphorylation, the right lateral optic nerve (LON) of each experimental animal was cut as described previously (*27*) (Figure. 1A). Recall that the axons of neurons activated by a central circadian clock reach the lateral eye (LE) by projecting through the LON (*22*, *29*). Therefore, by cutting the right LON we eliminated clock input to the right LE. The LON to the left LE was left intact; thus, the left LE received normal clock input.

The clock-driven efferent neurons innervating the eyes begin to fire action potentials around dusk, and they remain

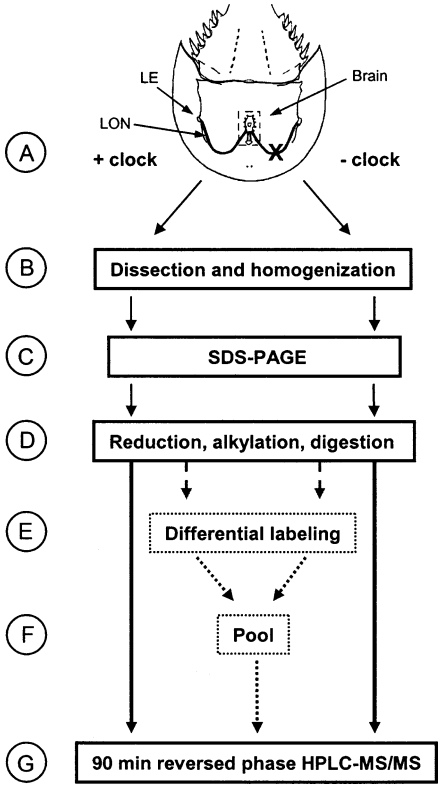

FIGURE 1: Schematic of both label-free and differential labeling experiments. Dashed arrows and boxes show additional steps associated with the differential labeling method only. (A) Circadian signals originate in the brain and reach the lateral eyes (LE) through the lateral optic nerve (LON). The LON to one eye of each experimental animal is severed (X) one week prior to extraction. This eye is the (−) clock eye. The eye with the intact optic nerve is referred to as the (+) clock eye. (B) The retinas from the (+) clock and (−) clock eyes were dissected from the animals and homogenized separately under infrared illumination, and high speed soluble fractions were concentrated as described in Experimental Procedures. (C) Concentrated soluble fractions were separated on SDS-PAGE gels and the location of LpMYO3 was visualized with Commassie Blue stain. (D) The LpMYO3 protein bands were cut from the gels, processed, and digested with trypsin as described in Experimental Procedures. Digests were extracted from the gel and dried. For label free analysis, the work flow proceeds directly to step G (solid arrows). Sample volumes were adjusted after drying for repeated LC-MS/MS analysis. For differential labeling analysis, the work flow includes E and F (broken arrows). (E) After digests were dried completely, they were differentially labeled by methyl esterification of carboxyl groups with either normal (d0) or deuterated (d3) methanolic HCl and then pooled (F). (G) Labeled samples are run in triplicate by LC-MS/MS as described in Experimental Procedures.

active throughout the night. The firing rate of these neurons slows as dawn approaches and then stops shortly after dawn (*46*, *47*). Therefore, at dusk on the day of the experiment, animals were moved into an aquarium located in a dark room, and unless otherwise stated, all subsequent manipulations were done under infrared illumination. Between 11 PM and midnight, when clock-driven efferent nerves are active and retinal sensitivity is high (*46*, *47*), both lateral eyes were dissected from the animals and excess tissue was removed from the back of the eye (Figure. 1A). A long section of the LON was often removed together with the eye that had the intact LON. Typically, this was cut from the back of the eye and discarded. However, in some experiments LON tissue was collected and processed in the same way as the LE to obtain gel-purified LpMYO3 for MS analysis. LON and LE tissues were always processed separately, and retinas from eyes with cut optic nerves [(−) clock input] and intact optic nerves [(+) clock input] were processed separately. Each sample contained one retina or LON from three or four different animals.

Samples were homogenized under infrared illumination in a MOPS buffer containing phosphatase inhibitors, protease inhibitors, and reducing agents (*43*), then centrifuged for 20 min in the dark at 120 000*g* in an Airfuge (Figure 1B). Subsequent processing occurred in ambient light. Supernatants obtained from the high-speed centrifugation were filter concentrated using 30 kDa cutoff membranes (Millipore) and denatured with SDS sample buffer. Extracts of the (−) clock input and (+) clock input LE samples and the LONs were loaded onto different 7.5% Tris-glycine SDS-PAGE gels poured from the same prepolymerized mixture and run at 150 V for 1 h. Gels were stained with Coomassie Blue for 5 min with shaking and were destained for approximately 5−6 h in a 10% glacial acetic acid (HAc)/10% methanol (MeOH) solution (Figure 1C).

LpMYO3 Digestion. The stained bands corresponding to LpMYO3 were excised from the gel, cut into 1 mm cubes, destained with gentle shaking in 50% acetonitrile (ACN)/50 mM ammonium bicarbonate (ABC) and subjected to in-gel digestion with trypsin according to a protocol used by the University of Florida's Interdisciplinary Center for Biotechnology Research (ICBR) Proteomics Core Facility (Gainesville, FL). Approximately 200 ng of trypsin in 50 mM ABC was added per single lane of gel band. Digestion was allowed to proceed for 17 h at 37 °C. Peptides were extracted by incubating gel pieces in a solution of 50% ACN and 5% formic acid until the gel pieces began to turn white. The supernatants were then removed and dried (Figure 1D). Some samples were dried completely and esterified as described below for differential labeling assays (Figure 1E−G). Alternatively, for label-free analysis, the supernatants were dried to near completion and resuspended in a solution containing 5% ACN and 0.1% HAc and analyzed (Figure 1D,G).

Methyl Esterification. Differential Labeling. Anhydrous methanol was purged with nitrogen for 5 min prior to use. The two labeling solutions [light (d0) and heavy (d3)] were prepared immediately prior to use by addition of 45 μL of thionyl chloride to 1 mL of either anhydrous methanol-d_0 (CH_3OH) or methanol-d_3 (CD_3OH). One milliliter of the appropriate labeling solution was added to peptides extracted from eight gel bands immediately after the peptides were completely dried. Tubes were blanketed with nitrogen, sealed, sonicated for 10 min, and allowed to stand at room temperature for 2 h. Reaction mixtures were then dried to near completion under vacuum, and labeled peptide digests were resuspended in a solution containing 5% ACN and 0.1% HAc. Samples to be compared were pooled, and the final volume was adjusted for repeated LC-MS/MS analysis (Figure 1G).

Liquid Chromatography (LC)-MS/MS Analysis. Validation of *in vivo* phosphorylation sites was achieved using a quadrupole ion trap MS (LCQ Deca MS, ThermoScientific, San Jose, CA) in line with a 5 cm × 75 μm inner diameter (i.d.) Pepmap C18 5 μm/300 Å capillary column (LC Packings, Sunnyvale, CA) or a self-packed 10 cm × 75 μm i.d. Altima 5 μm/300 Å capillary column (Alltech Associates,

Inc., Deerfield, IL). An HPLC system composed of two independent Applied Biosystems 140 pumps and a Perkin-Elmer Series 200 autosampler, with a 1/30 precolumn split from the analytical pump, was used to deliver a 60-min gradient from 5% to 50% mobile phase B (mobile phase A = 0.1% HAc, 0.01% TFA, 3% ACN; mobile phase B = 0.1% HAc, 0.01% TFA, 95% ACN) at a flow rate of 12 μL/min. Parent ion scans were followed by four data-dependent MS/MS scans. For targeted analysis, one data-dependent MS/MS scan and two to three single ion monitoring (SIM) scans followed the parent ion scan. SIM scans were dedicated to isolating and fragmenting ions with a mass corresponding to specific, suspected phosphopeptide ions over the entire course of the chromatogram. Tandem mass spectra from the raw data of these experiments were extracted by Bioworks Browser version 3.0 and subsequently searched against the NCBI (National Center for Biotechnology Information) number database using the Mascot version 1.9 search engine. In these searches, the taxonomy specified was metazoa, trypsin was identified as the cleavage enzyme, and carbamidomethylation was defined as a fixed modification. Serine/threonine phosphorylation and methionine oxidation were selected as variable modifications. Mass tolerances were set to 2 Da for MS and 1 Da for MS/MS. Extracted ion chromatograms (EICs) were constructed to locate eluting phosphopeptides based on the ion current of peaks in the MS/MS spectra resulting from the neutral loss of 98 Da (H_3PO_4) from the parent ion. For SIM experiments, EICs were constructed based on total ion current in the MS/MS spectra measured during each individual SIM scan event. The mass of the peptide produced by neutral loss of 98 Da (H_3PO_4) from the targeted parent ion was added into the filter criteria for EIC construction.

Both label-free and differential labeling quantitative analyses were conducted using a hybrid quadrupole time-of-flight mass spectrometer (QSTAR XL MS, Applied Biosystems, Foster City, CA) interfaced with an Ultimate Capillary HPLC system (LC Packings, Sunnyvale, CA) operated at a flowrate of 180 μL/min with a 1/1000 precolumn split. This integrated system delivered a 90 min gradient from 3% to 40% mobile phase B (mobile phase A and B as described above) through a 15 cm $\times$ 75 μm i.d., 5 μm/300 Å PepMap C18 capillary column (LC Packings, Sunnyvale, CA). All samples were run in triplicate, and three to four blanks were run between the different label-free sample sets to prevent carry over. One survey scan followed by one to three information dependent MS/MS scans was performed. Data were extracted using Analyst version 1.1 and searched using Mascot with the settings given above except for the following: mass tolerances was set to 0.3 Da for MS and 0.3 Da for MS/MS, and in the differential labeling experiments, methyl esterification at the C-terminus and at acidic residues was set as a variable modification. Defining methyl esterification as a variable modification facilitated the detection of nonlabeled or inefficiently labeled myosin peptide product. The first two isotope peaks of the average mass spectrum for each ion of interest were integrated for quantitative analysis.

Validation of Quantification Methods. The methyl esterification reaction used for differential labeling was tested for reaction efficiency by performing the reaction on a simple mixture of synthetic phosphopeptides and assaying by MS for mass shifts of the peptide ions equivalent to the addition of the mass of one methyl group. To test for equal labeling efficiency with both regular (d0) and deuterated (d3) methanol, aliquots of tryptic peptides from expressed Lp-MYO3 were labeled with d0- or d3-methanol, pooled in a 1:1 and 1:2 ratio and analyzed by HPLC-MS/MS. The area ratios of the nonoxidized, phosphorylated peptide RSpS^{846}-IQENMLLPER, and control peptides VLPLYGDQTAVK, SDNPPHVFAVADR, and YYSEEYLSR were compared to their expected values. Additionally, to identify nonreacted or incompletely reacted peptide byproduct from LpMYO3 tryptic digests, all experimental data files were searched using Mascot with C-terminal and aspartic or glutamic acid methylation listed as a variable modification (as described in Experimental Procedures).

The label free method for quantification was validated by creating and assaying standard samples that mimicked the biological samples to be analyzed. Specifically, different quantities of one of two synthetic phosphopeptides (RSp-SIQENMLLPER or KKSVpSTPF) were added to aliquots of a tryptic digest of BSA to create four standard samples for each phosphopeptide with each sample containing a unique ratio of phosphopeptide to BSA peptides. All samples were analyzed four times by LC-MS/MS, and the signals corresponding to the phosphopeptides and three BSA peptides were integrated. One of the four peptide mixtures containing each phosphopeptide (Sample 2, for example) was chosen arbitrarily as the "control" sample, and signal intensities for each peptide analyzed from the other samples were compared to the signal intensities of the same peptides in Sample 2. Average BSA peptide ratios were determined for each sample comparison (Sample 1 to 2; Sample 3 to 2; Sample 4 to 2), and these values were used to normalize the measured phosphopeptide ratios obtained in each sample. The normalized phosphopeptide ratio in each sample was then plotted against the theoretical ratios calculated from the actual molar quantities of components in the solutions.

Interpretation of the Differential-Labeling Data. EICs were generated for both d0- and d3-labeled versions of all peptides studied. Mass spectra were averaged over the elution profile of each d0- and d3-labeled peptide pair to account for chromatographic shifts resulting from differential labeling. As is illustrated in Figure 2, the first two isotope peaks of each isotopic cluster were integrated using Applied Biosystems' Analyst software, and areas of peaks associated with the same peptide were summed. The area values from each of three runs were then summed to obtain a total area value for each peptide for each set of animals. To obtain the 'raw' (+) clock/(−) clock ratio, the total area of peaks corresponding to each peptide from retinas in the (+) clock cell state was divided by the total area of peaks corresponding to the same peptide from retinas in the (−) clock cell state. This calculation was performed for each phosphopeptide studied. Similar (+) clock/(−) clock ratios were also obtained for four control peptides, nonmodified peptides derived from LpMYO3 that contained at least one acidic residue. The (+) clock/(−) clock ratios obtained for the four control peptides were averaged to obtain a factor that was used to normalize the (+) clock/(−)clock ratio obtained for the phosphopeptides, and thus control for any differences in retinal tissue collection, tissue homogenization, LpMYO3 extraction,

$$\frac{+\text{ clock}}{-\text{ clock}} = \frac{(d0_1) + (d0_2)}{(d3_1) + (d3_2)}$$

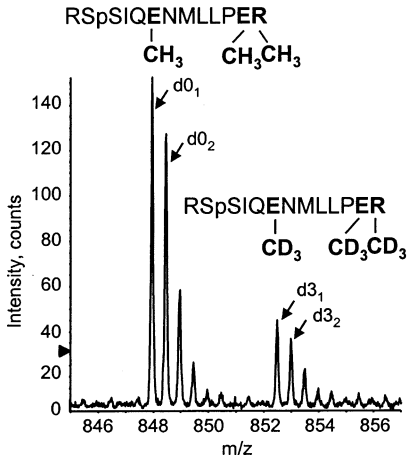

FIGURE 2: Sample determination of the raw of (+) clock to (−) clock ratio using differential labeling and the peptide shown. In this example, LpMYO3 peptides from (+) clock eyes and (−) clock eyes were labeled by methyl esterification with normal (d0) or deuterated (d3) methanol, respectively. The first isotope cluster is from the d0-labeled phosphopeptide while the second cluster is from the d3-labeled phosphopeptide. All acidic residues and C-terminal residues (bold) were labeled by conversion of carboxylic groups to methyl esters. All parent ion scans across the elution profile of both phosphopeptides in each pair were summed to generate a representative spectrum of each pair and thus account for chromatographic shifts in differentially labeled peptides. To calculate a (+) clock to (−) clock ratio, the first two isotope peaks (arrows) from each isotope cluster ($d0_1$ and $d0_2$, or $d3_1$ and $d3_2$) were integrated and the areas of each peak were summed [$(d0_1) + (d0_2)$]. The summed areas from the (+) clock phosphopeptide was divided by the summed area from the (−) clock phosphopeptide to obtain a raw (pre-normalization) ratio. The raw ratios were subsequently normalized to ratios obtained with control nonphosphorylated peptides as described in Experimental Procedures and shown in Table 1A−D. m/z, mass-to-charge ratio.

digestion, labeling, and any other discrepancies in sample handling prior to pooling.

Since all individual control peptide ratios should theoretically be equal, the relative 95% confidence interval obtained from control peptide ratios during the determination of the normalization factor was considered the error introduced by the method. The normalized (+) clock/(−) clock ratio for each phosphopeptide was multiplied by the relative 95% confidence interval (determined from the control peptide ratios) to determine the error in each measurement for each experiment. Final (+) clock/(−) clock ratios are the calculated change in phosphorylation at each site in response to circadian clock input determined by averaging values obtained from experiments using three different sets of animals. The error reported in this final value, which represents biological variation, is the 95% confidence interval determined from these averaged values.

Interpretation of the Label-Free Data. The (+) clock/(−) clock ratios for phosphopeptides assayed with the label- free technique were calculated and normalized as described for the differentially labeled data sets except that six control peptides were measured. The error for each experiment was also defined as described for the differential labeling sets. Tables 1A−D presented in Supporting Information show sample calculations for a label-free experiment. Table 2 in the Supporting Information shows the calculations used to determine the methodological and biological errors for both the differential labeling and label-free experiments.

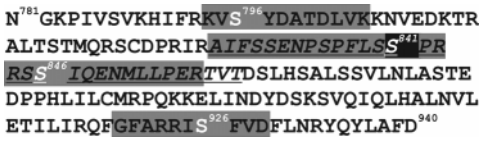

FIGURE 3: Sequence of the predicted loop 2 region of LpMYO3 showing all phosphopeptides (highlighted in gray) and phosphorylation sites (serines in white) identified by MS. Loop 2 is in italics. Serines shown in white on gray are substrates for PKA and autophosphorylation; the one serine boxed in black is not phosphorylated by PKA or autophosphorylation, but is a predicted substrate for PKC. The first three sites, S^{796}, S^{841}, and S^{846}, were identified in both recombinant LpMYO3 (*19*) and native LpMYO3 (Figures 4−6) while the most C-terminal site, S^{926} was identified only in native protein originating from the LON (Figures 5 and 7).

RESULTS

Quantification of LpMYO3 in Soluble Fractions of LE and LON. The current studies of endogenous LpMYO3 in photoreceptors were facilitated by the high concentration of LpMYO3 in soluble extracts of *Limulus* LE and LON: 2.4 ± 0.3% and 5.8 ± 0.4% respectively of total soluble proteins as averaged from three separate determinations. Previous analyses of soluble extracts of LE and ventral photoreceptor proteins showed that LpMYO3 migrates as a prominent Coomassie Blue stained band on SDS PAGE gels with an apparent molecular mass of 122 kDa (see, for example, ref 19). Two-dimensional studies showed further that this band contains a single protein (*27*).

Identification of in Vivo LpMYO3 Phosphorylation Sites. Three phosphorylation sites, S^{796}, S^{841}, and S^{846}, were identified in previous mass spectrometric analyses of baculovirus-expressed LpMYO3 that had been phosphorylated *in vitro* with PKA (*19*) (Figure 3). These same three phosphorylation sites were identified in analyses of endogenous LpMYO3 using the LCQ Deca MS (Figure 4A, 4B, 5B, 5D). Phosphorylated peptides containing either S^{841} or S^{846} were identified by standard data dependent LC-MS/MS experiments. Both phosphorylated serines are located within loop 2: S^{846} is a known substrate for PKA (*19*); S^{841} is a predicted PKC substrate (*49*).

Phosphorylated peptides containing S^{796}, a known PKA substrate in the expressed protein, and S^{926}, a predicted PKA site that can be autophosphorylated in the expressed protein (*19*), were not identified in data-dependent experiments. Rather, a targeted analysis (single ion monitoring) using the LCQ Deca MS was required to identify these phosphopeptides. Figure 5A shows the base peak chromatogram from one experiment using LpMYO3 from LON. The selected ion chromatograms for these peptides are shown in Figures 5B and 5C, and the MS/MS spectra are presented in Figures 5E and 5F. All the phosphopeptides detected in LpMYO3 from the LE were detected in the protein extracted from the LON. Interestingly, an additional phosphopeptide containing S^{926} was found in LpMYO3 extracted from the LON. The MS/MS spectra generated from the targeted experiments demonstrated the characteristic predominant neutral loss fragment ion of both phosphopeptides ($M + 2H - H_3PO_4$) in addition to one or more additional fragment ions. Nevertheless, the

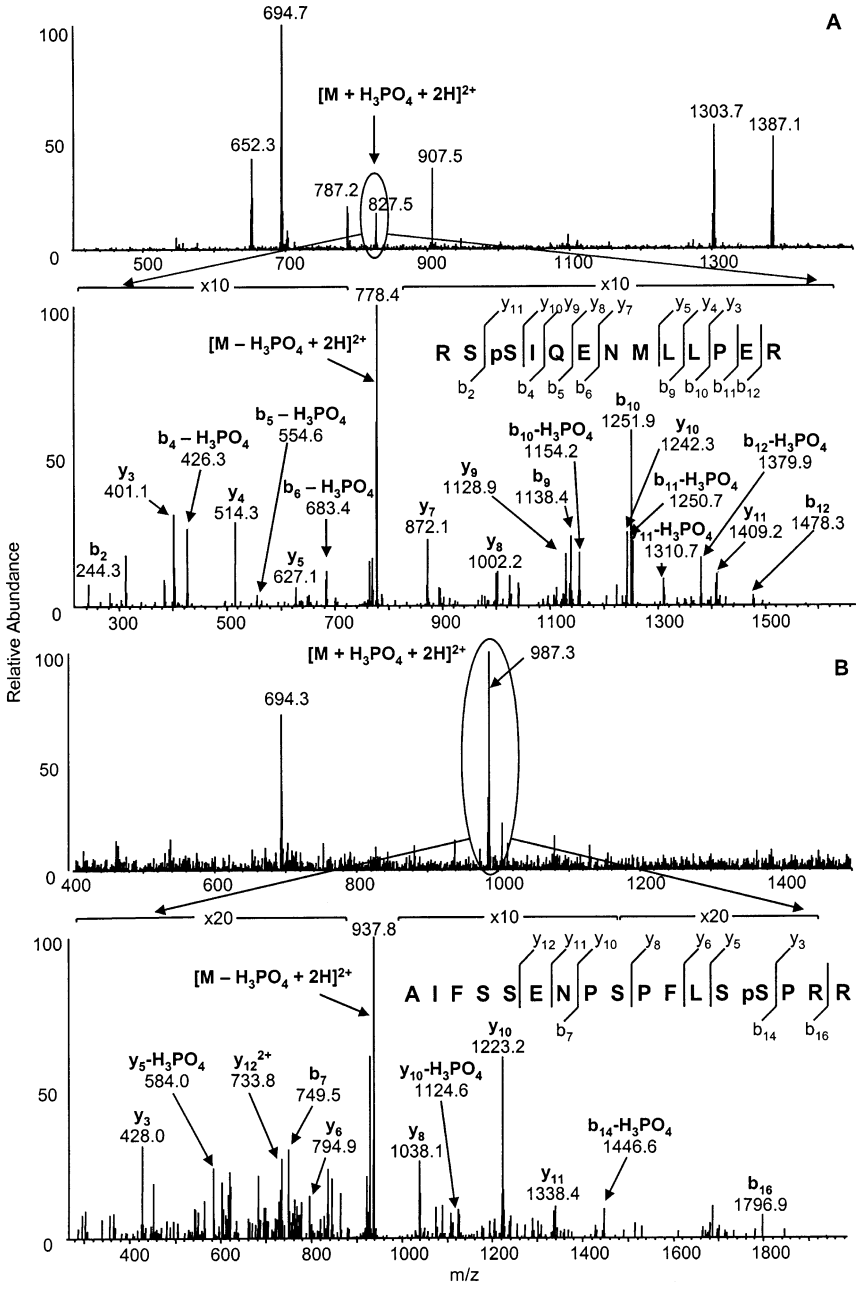

FIGURE 4: MS/MS verification of the two most easily detected phosphopeptides found in LpMYO3 *in vivo*: (A) RSpS[846]IQENMLLPER, (B) AIFSSENPSPFLSpS[841]PR. MS/MS spectra are labeled according to the Beimann (*48*) model for peptide fragmentation. Both peptides were identified by data dependent MS/MS using the LCQ Deca ion trap mass spectrometer. A and B, upper panels: survey scans from which the ion was chosen for fragmentation. The phosphorylated parent ion is circled. A and B, lower panels: MS/MS spectra for the ion located by neutral loss filtering postacquisition. The area surrounding the prominent ion resulting from neutral loss of the phosphate group is magnified by a factor of 10 or 20 as is indicated on the figures.

relatively low signal-to-noise ratio of these MS/MS spectra warranted further verification of these results. Using the QSTAR XL MS, phosphorylation at S[796] was supported by the observation of coeluting peaks that matched the +2 and +3 charge state of this phosphorylated, tryptic peptide with high mass accuracy (~5 ppm for the +2 charge state) (Figure 6). MS/MS of the peptide containing phosphorylated S[926] obtained by qTOF-MS confirms the ion trap assignment of phosphorylation at this site (Figure 7). Importantly, all of the phosphorylation sites identified in the expressed protein were identified in the endogenous protein and all are within or near loop 2.

Validation of Quantification Methods. The two approaches used to quantify the influence of the circadian clock on the relative levels of phosphorylation at each phosphorylation site in LpMYO3, a differential isotope labeling approach using methyl esterification and a label-free approach, were validated in preliminary experiments.

When the methyl esterification reaction was performed on a simple mixture of synthetic phosphopeptides, the spectra obtained before and after the reaction demonstrated a mass shift of all peptide ions equivalent to the addition of the mass of one methyl group. No nonreacted peptide by-product was detected, suggesting the reaction is highly efficient (data not shown). When aliquots of tryptic peptides from expressed LpMYO3 were labeled with d0- or d3-methanol, pooled in a 1:1 and 1:2 ratio, and analyzed by HPLC-MS/MS, the average area ratios of the nonoxidized,

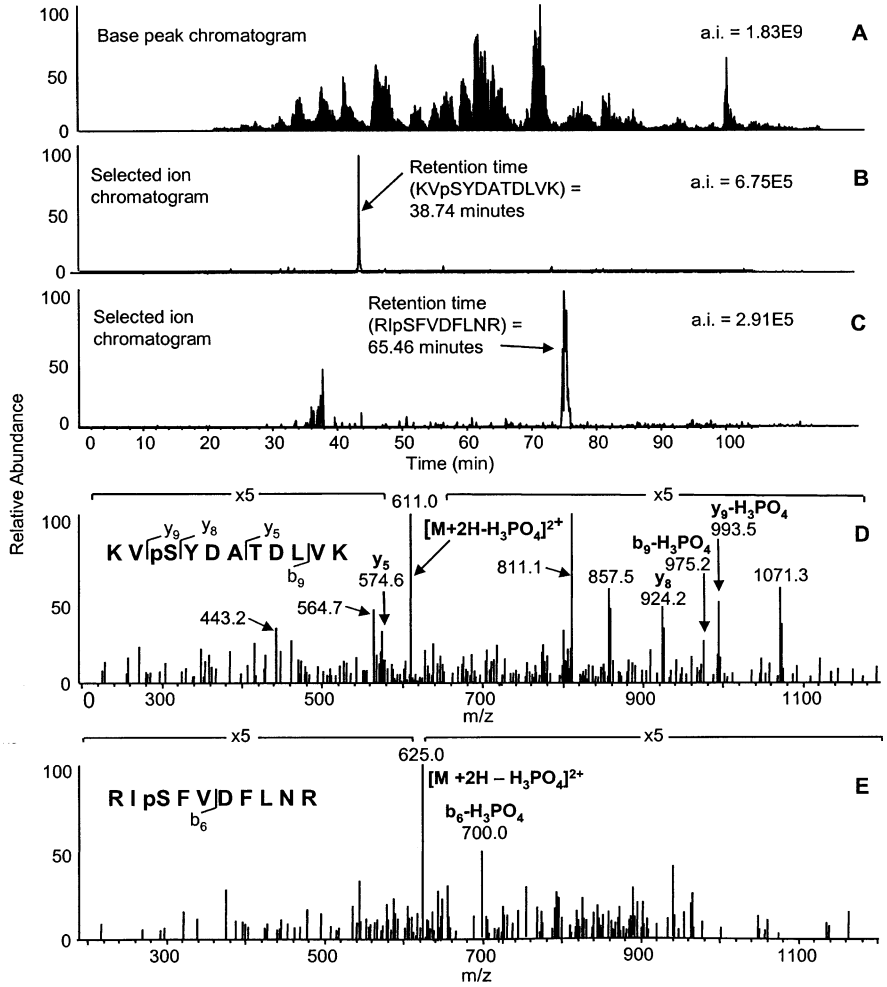

FIGURE 5: MS/MS verification of two additional phosphorylation sites in LpMYO3 using the LCQ Deca MS. These sites were not identified by data-dependent analysis. (A) Base peak chromatogram for the targeted data dependent analysis of LpMYO3 from the LON. (B and C) Selected ion chromatograms for KVpS[796]YDATDLVK and RIpS[926]FVDFLNR, respectively, identified by single ion monitoring. The absolute intensity (a.i.) is noted in the upper right-hand corner of chromatograms in A−C. (D and E) MS/MS spectra for KVpS[796]YDATDLVK and RIpS[926]FVDFLNR, respectively. The area surrounding the prominent ion resulting from neutral loss of the phosphate group is magnified by a factor of 5. MS/MS spectra are labeled as in Figure 4.

phosphorylated peptide RSpS[846]IQENMLLPER and control peptides VLPLYGDQTAVK, SDNPPHVFAVADR, and YYSEEYLSR were within 20% of their calculated values. This indicated similar reaction efficiencies for heavy and light labeling schemes. Finally, our search of all experimental data for nonreacted or incompletely reacted peptide byproduct from LpMYO3 tryptic digests with Mascot using C-terminal and aspartic or glutamic acid methylation listed as a variable modification (as described in Experimental Procedures) produced no evidence for incomplete peptide labeling over the course of this work.

To validate the label-free method for quantification, we added different amounts of one of two phosphopeptides to aliquots of a standard mixture of tryptic peptides of BSA so that each resulting sample contained a unique ratio of phosphopeptide to BSA peptides (Figure 8, upper panel). All samples were analyzed by LC-MS/MS. The ratio of phosphopeptide peak areas (determined as described in Experimental Procedures) in samples 1, 3, and 4 to that in sample 2 (arbitrarily selected as the control sample) were normalized using the average ratio of BSA peptide peak areas in samples 1, 3, and 4 to that in sample 2. The lower panel of Figure 8 shows these values plotted against the theoretical ratios calculated from the actual molar quantities of components in each sample. Linear regressions with slopes close to 1 with *y*-intercepts near 0 were obtained for each phosphopeptide, indicating a close correlation of the measured and calculated values. These findings validate the use of the label-free method for quantifying differences in phosphorylation levels of an individual peptide obtained from two different biological samples.

Changes in Levels of Phosphorylation in Response to Clock Input. Using the differential labeling method, phosphorylation changes could be measured only at phosphorylation sites, S[841] and S[846]. The average (+) clock/(−) clock ratios obtained were 0.96 ± 0.27 for S[841] and 1.97 ± 0.28 for S[846]. Ratios were calculated from three independent labeling experiments performed with three different sets of animals (Figure 9), and each set contained tissue pooled from three to four animals. Furthermore, the values determined for each group of animals represent the sum of at least three independent LC-MS/MS runs. These results show that the phosphorylation of S[846] increases nearly 2-fold in response to signals from the circadian clock while the level of phosphorylation of S[841] is unchanged. The errors reported with the average normalized value represent the 95% confidence interval of normalized ratios obtained from experiments with three different sets of animals and describe

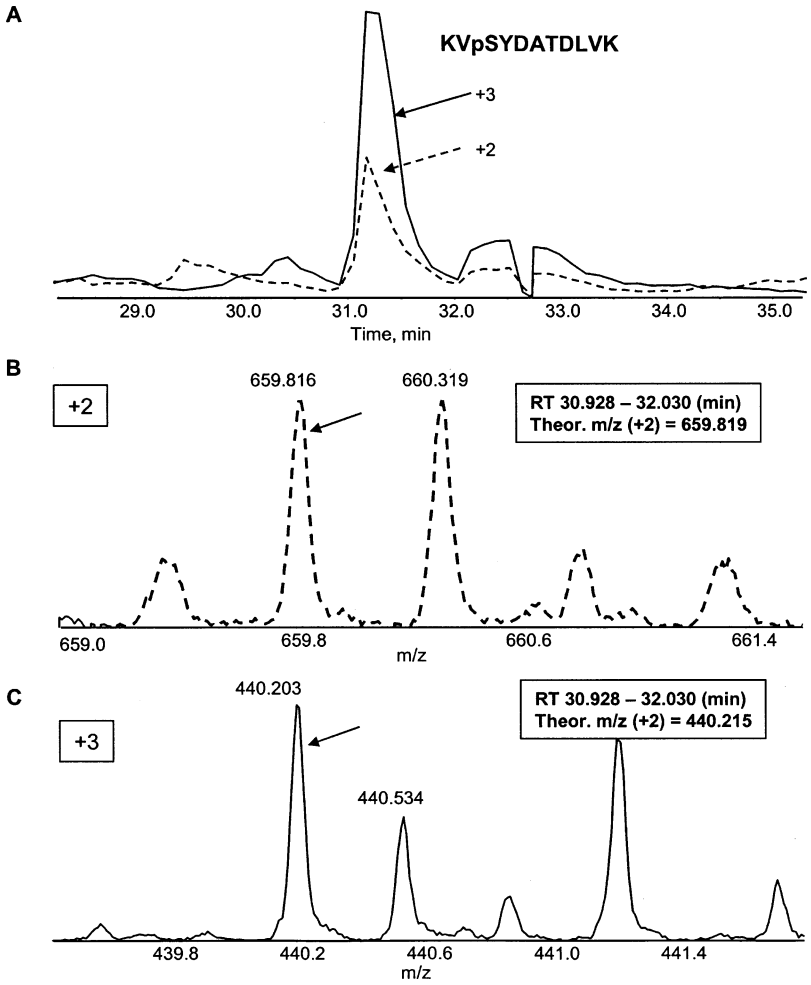

FIGURE 6: Additional verification of phosphorylation at S^{796} using the QSTAR XL hybrid quadrupole time-of-flight mass spectrometer. A: superimposed selected ion chromatograms of the masses corresponding to the +2 and +3 charge state of KVpS^{796}YDATDLVK. Coelution of these masses suggests their relationship to the same peptide. B and C: MS spectra of the +2 and +3 charge states of this peptide, respectively. The experimentally determined mass/charge ratios (*m*/*z*) of the first two peaks in each charge state are shown. The theoretical mass/charge ratio for the monoisotopic peak (arrows) in each charge state is presented in the boxes for comparison.

the biological variation between sample sets. The average relative 95% confidence intervals determined from control peptide ratios for differential labeling was 9.7%, indicating the error introduced by the method within each experimental set.

During the analyses of sample set 3, the LpMYO3 from each set of eyes was labeled in both configurations [d0-labeled (+) clock, d3-labeled (−) clock; d3-labeled (+) clock, d0-labeled (−) clock] to test, once again, whether the labeling step contributed to the final ratio. Values obtained from both labeling configurations were similar, and thus raw data were summed to determine a single set of values for this animal set.

The label-free approach produced results consistent with data from the labeling experiments (Figure 10). In addition, we were able to measure changes in the levels of phosphorylation at S^{796}. Three label-free analyses based on three different groups of animals were completed, yielding an average (+) clock/(−) clock ratio at S^{796} of 2.39 with a 95% confidence interval of 0.73. As with the differential labeling method, each group of animals tested consisted of LpMYO3 obtained from one retina pooled from three animals, and the (+) clock/(−) clock ratio of S^{796} for each experiment was determined from the summed integrated peak areas from at least three independent LC-MS/MS analyses. Although the average relative 95% confidence interval generated within each experiment by the label-free method (17.9%) was greater than that generated by the differential labeling approach, the label-free approach was more sensitive than the differential labeling technique, permitting detection of changes in the phosphorylation of S^{796}.

After combining data obtained from assays performed with the differential labeling and label-free methods, the (+) clock/(−) clock phosphorylation ratios for $S^{841}$and S^{846} are, respectively, 0.94 ± 0.12 (95% CI), and 1.84 ± 0.24 (95% CI) (Figure 11). These values represent the average from six independent measurements. The final (+) clock/(−) clock ratio for S^{796} is 2.39 ± 0.73. This represents the average of three independent experiments in which the samples were processed for label-free analysis. These data demonstrate a statistically significant and reproducible elevation in phosphorylation at two PKA phosphorylation sites, S^{796} and S^{846}, in response to circadian clock input. In contrast, no clock-driven change in level of phosphorylation was observed at S^{841}, the putative PKC site. No clock-driven change in the level of phosphorylation at S^{926} was measured as no phosphorylation at this site was detected in extracts of the LE retina by either method.

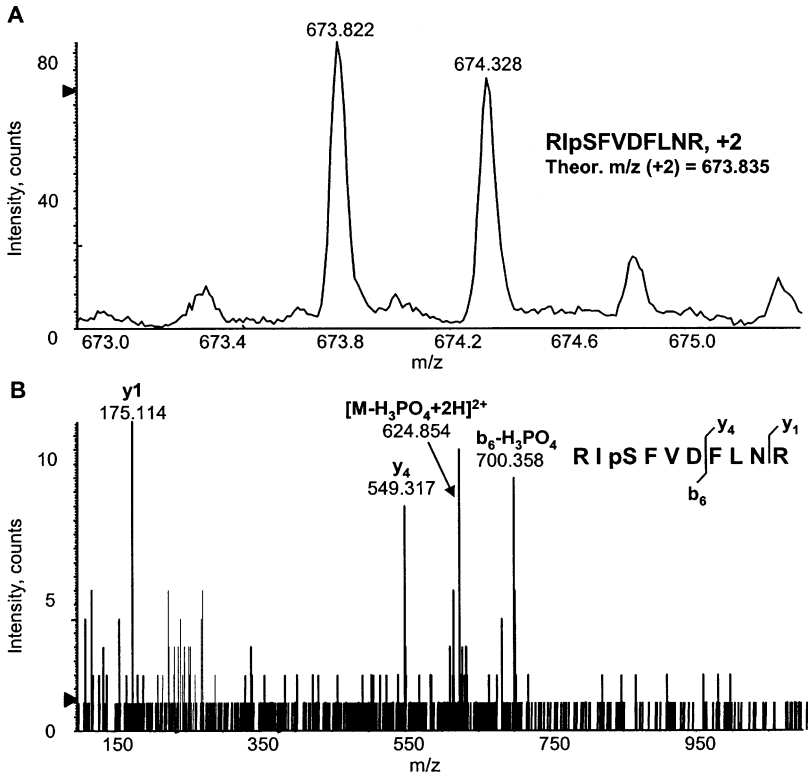

FIGURE 7: Additional MS/MS verification of phosphorylation at S^{926} on LpMYO3 derived from the LON using the QSTAR-MS. A: Full MS of the +2 charge state of RIpS^{926}FVDFLNR. The theoretical monoisotopic mass/charge ratio (*m*/*z*) of this peptide is shown in the box. B: MS/MS spectrum of this peptide labeled as in Figure 4.

DISCUSSION

This study reports two major findings: (1) LpMYO3 extracted from *Limulus* LE is phosphorylated at three sites within the loop 2 actin binding interface of its myosin domain: S^{796}, $S^{841}$and S^{846}, and (2) natural clock input enhances by roughly 2-fold the phosphorylation of two PKA sites, S^{796} and S^{846}. The phosphorylation sites were identified by standard HPLC-MS/MS methods; changes in phosphorylation levels were measured with two different quantitative methods.

Comparisons of the Methods Used To Measure Changes in Phosphorylation. A comparison of the two methods used to quantify changes in phosphorylation, differential labeling by methyl esterification, and label-free relative quantification, shows that the label-free method has some clear advantages. Only the two most easily detected phosphorylation sites, S^{841} and S^{846}, were detected in the differential labeling assays. However, in label-free analyses, phosphorylation at S^{796} was detected consistently in both the (+) clock and (−) clock cell states, permitting us to quantify changes in its level of phosphorylation. The limitation to the sensitivity of the differential labeling by methyl esterification method is attributed to sample loss during the multiple sample drying steps required for efficient labeling.

The label-free method of analysis also has disadvantages. The instrument time required is at least triple that of the differential labeling method since samples are not pooled and blanks are required in between analysis of samples from different cell states. Also, the average relative 95% confidence interval of the control peptides determined from label-free analyses was nearly double that determined from differential labeling analysis. However, this increased variation may be influenced by other noncontrolled factors, since differential-labeled and label-free analyses were performed at different times and with different animal sets.

Identification of in Vivo Phosphorylation Sites on Endogenous LpMYO3. Three of the phosphorylation sites found in endogenous LpMYO3 extracted from the LE and LON, S^{796}, S^{841} and S^{846}, were previously identified by HPLC-MS/MS in baculovirus expressed LpMYO3 after *in vitro* PKA phosphorylation (*19*). A fourth phosphorylation site, S^{926}, was identified only in endogenous LpMYO3 extracted from the LON. Our previous studies showed that although S^{926} is a predicted PKA phosphorylation site, it is not phosphorylated by PKA *in vitro* in the expressed protein, and it is a poor substrate for autophosphorylation by full-length LpMYO3 (*19*). Thus, in endogenous LpMYO3, the level of S^{926} phosphorylation is probably low and the result of autophosphorylation or the phosphorylation by an as yet unidentified kinase.

Our failure to detect phosphorylated S^{926} in LpMYO3 extracted from the LE could reflect a biological difference between LpMYO3 located in the LE and the LON. Alternatively, it may be the result of the different protein levels in these tissues combined with the sensitivity limits of the methods used or poor ionization efficiency in ESI. As we showed, the concentration of LpMYO3 in LON extracts is higher than that in LE extracts. Future enhancements in method sensitivity may enable the semiquantitative analysis of phosphorylation at this site in LpMYO3 from the LE.

Measurement of Site Specific Changes in Phosphorylation in Vivo in Response to Circadian Clock Input. Of the four phosphorylation sites identified in endogenous LpMYO3 only two, S^{796} and S^{846}, showed statistically significant and

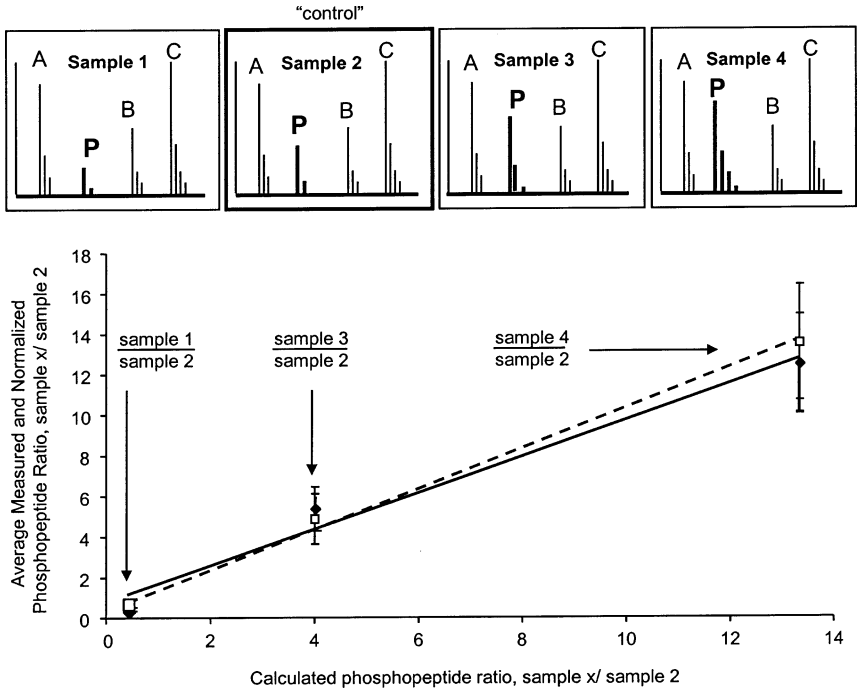

FIGURE 8: Evaluation of the label-free relative quantification method with four standard peptide mixtures. Upper panel: Schematic showing the preparation of four standard peptide mixtures containing a fixed concentration of a BSA tryptic digest and a different concentration of a synthetic peptide (P). Two different synthetic phosphopeptides were assayed, RSpSIQENMLLPER and KKSVpSTPF. Peak areas for three BSA peptides (A, B, and C) and the added phosphopeptides (P) were determined in each sample using the QSTAR XL MS. From these data, a normalized phosphopeptide ratio was determined for each sample as described in Experimental Procedures using Sample 2 as the "control" sample. Lower panel: The experimentally determined normalized phosphopeptide ratio obtained for each sample relative to that in Sample 2 is plotted against the calculated ratios determined from the known number of moles of each phosphopeptide added to each sample. These assays were repeated four times for each phosphopeptide and the mean ± the standard deviations are plotted. Plots with slopes close to one indicate a good correlation between the actual and measured ratios and validate the use of this technique for relative quantification.. RSpSIQENMLLPER:(◆◆) Slope = 0.90 and R^2 value = 0.978. KKSVpSTPF (□□) Slope = 1.00 and R^2 value = 0.996.

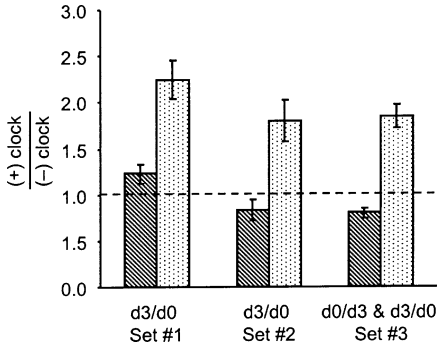

FIGURE 9: Normalized (+) clock to (−) clock ratios calculated from three independent animal sets via differential labeling. Phosphopeptides containing S^{841} and S^{846} were identified for quantification. An approximate 2-fold elevation in phosphorylation at S^{846} (spotted bars) was detected in each sample set in response to clock input while no change was detected for S^{841} (striped bars). Results reported in data set 3 were obtained by averaging ratios from sample sets labeled in both configurations, (+clock [d0]/-clock [d3]) and (+clock [d3]/-clock [d0]). Error bars represent the 95% confidence interval determined from four control peptides in each experimental set and indicate the error introduced by the method. The dashed line at a +clock/-clock ratio of 1.0 denotes the ratio of no change.

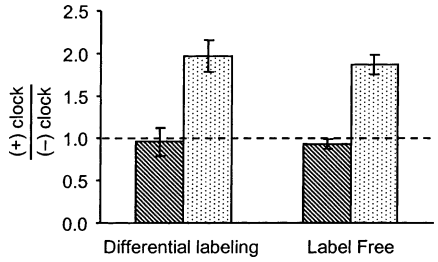

FIGURE 10: Comparison of average normalized (+) clock/(−) clock ratios obtained from differential labeling and label-free experiments for S^{841} (striped bars) and S^{846} (spotted bars). Each method was applied to LpMYO3 obtained from the eyes of three separate sets of animals, and animal sets used for the differential labeling and label free experiments were different from one another. Error bars represent the average 95% CI determined from the normalized phosphopeptide ratios calculated from each set. This error indicates the amount of biological error observed between different animal sets processed by each method. The dashed line at the (+) clock/(−) clock ratio of 1.0 denotes the ratio of no change. The two different methods produced similar results.

reproducible changes in their phosphorylation levels in the LE in response to clock input *in vivo*, and both sites demonstrated a roughly 2-fold increase in phosphorylation. It should be emphasized that the 2-fold change in the phosphorylation of S^{846} was observed with both differential-labeling and label-free techniques.

Both clock-regulated phosphorylation sites are known substrates for PKA in baculovirus-expressed LpMYO3 (*19*). Interestingly, the level of phosphorylation at S^{841}, a putative PKC site, did not change in response to clock input. These findings suggest that the changes in phosphorylation we observe are specific, and they are consistent with previous results showing that OA, the neurotransmitter released from the clock-driven neurons innervating the eyes, elevates cAMP in photoreceptors and activates PKA (*2*, *23*−*29*), while there is no evidence for clock activation of PKC in photoreceptors. Our current observations also confirm and extend the results

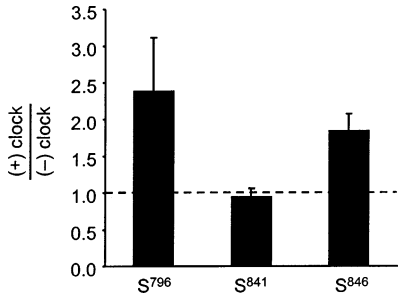

FIGURE 11: Final (+) clock to (−) clock ratios obtained for three phosphorylation sites indicating the degree to which phosphorylation changes in response to clock input. The average values for S^{841} and S^{846} were determined from six experiments (three differential labeling and three label-free analyses). The average value for S^{796} was determined from three label-free experiments. Error bars represent the 95% confidence interval of the ratios obtained from each experiment and indicated the degree of biological variation. The dashed line at a (+) clock/(−) clock ratio of 1.0 denotes the ratio of no change. An approximate 2-fold increase in phosphorylation is observed at S^{796} and S^{846} in response to clock.

of previous back-phosphorylation studies demonstrating a global increase in the phosphorylation of PKA sites in LpMYO3 *in vivo* in response to clock input (*28*). The identification of the exact sites regulated by clock input *in vivo* provided by the current study is critical for the design of future experiments examining the physiological consequences of clock-driven phosphorylation.

Our results show a roughly a 2-fold increase in phosphorylation at both the S^{796} and S^{846} sites, but they do not show the absolute levels of phosphorylation at each site. This measurement cannot be made with the available data due to unpredictable differences in the ionization efficiency of phosphorylated peptides and their nonphosphorylated counterparts. But with the phosphorylation sites that are regulated by clock input *in vivo* now clearly identified, this question can be addressed in future experiments. The 2-fold increase in phosphorylation observed may seem small. However, this increase was measured in LpMYO3 prepared from total cell homogenates. Since LpMYO3 is distributed throughout the photoreceptor, the increase we measured may greatly under estimate increases that take place in specific cell compartments, such as near the photosensitive membrane.

Significance of Enhanced Phosphorylation at S^{796} and S^{846} by Circadian Clock Input. One of the PKA sites influenced by clock input, S^{846}, is located within loop 2 of the myosin domain of LpMYO3, a known actin binding region of other myosins. The other site, S^{796}, is located on the N-terminal side of loop 2 within the actin binding cleft (*50*). In other myosins (*39*, *40*), as the net positive charge in loop 2 increases, actin affinity also increases both in the absence and presence of nucleotide. Therefore, we propose that a reduction in net charge in loop 2 via phosphorylation of S^{846} will decrease the affinity of myosin for actin. Phosphorylation of S^{796} may have a similar affect. However, since the primary sequences of the myosin head domain of LpMYO3 is among the least conserved, phosphorylation in its loop 2 region also may have unexpected functional consequences.

Comparisons with Other Class III Myosins. These studies provide the first identification of specific phosphorylation sites in any myosin within or near loop 2 *in vivo*. However, the phosphorylation of the myosin motor domain in this region may be characteristic of class III myosins. For example, although exact phosphorylation sites have not yet been identified, the baculovirus-expressed kinase domain of *Drosophila* class III myosin (NINAC) phosphorylates the short form of NINAC within either the myosin or tail domain (*16*). Furthermore, baculovirus-expressed HMYO3A autophosphorylates a peptide located near the C-terminus of the myosin motor domain that includes a portion of loop 2 (*17*). The functional consequences of the phosphorylation of NINAC and HMYO3A are not yet known, but recent studies with HMYO3A and fish MYO3A provide indirect evidence that either autophosphorylation of the myosin domain, or the presence of the kinase domain, reduces the affinity of the myosin for actin (*10*, *18*, *20*, *51*). These observations are consistent with our predictions based on the current study of LpMYO3.

Possible Functional Consequences of the Clock-Driven Phosphorylation at S^{796} and S^{846} for Limulus *Photoreceptors.* One major effect of the clock-driven phosphorylation of both S^{796} and S^{846} in LpMYO3 at night may be a nighttime reduction in the affinity of LpMYO3 for actin within the axial core of the photosensitive microvilli and a reduction in the concentration of LpMYO3 in the photosensitive microvilli. MYO3 in *Drosophila* photoreceptors (NINAC) is thought to stabilize the actin within the axial core of the photosensitive microvilli. NINAC typically binds to the actin in the photosensitive microvilli (*52*), and in *Drosophila* lacking NINAC, the actin within these microvilli is fragmented or missing even before eclosion (*53*). Thus, the clock-driven phosphorylation of sites within and near the loop 2 actin-binding interface of LpMYO3 lead us to propose that LpMYO3 phosphorylation participates in circadian processes involving changes in the stability of actin within the photosensitive microvilli. One such process is light-triggered transient shedding of photosensitive membranes which involves the rapid, light-triggered breakdown of the photosensitive microvilli and internalization of photosensitive membranes (*33*, *34*, *54*). This process may be partly responsible for rapidly converting the photoreceptors from a high to a low sensitivity state. Although triggered by light, transient membrane shedding must be "primed" by the activation of PKA in response to clock input (*35*, *36*). The clock-driven phosphorylation of S^{796} and S^{846} in LpMYO3 described here may contribute to this priming event.

The phosphorylation of S^{841}, the predicted PKC site also located within loop 2, may further reduce the affinity of LpMYO3 for actin and contribute to the light-trigger for transient shedding. Light-dependent phosphorylation of LpMYO3 has been described (*55*). Light is thought to activate PKC in arthropod photoreceptors (*56*, *57*), and in *Limulus*, the activation of PKC triggers shedding in photoreceptors previously "primed" by clock input (*58*)

The clock-driven phosphorylation of LpMYO3 may have other consequences. A clock-driven change in the affinity of LpMYO3 for actin could change the concentration of LpMYO3 at photosensitive microvilli and lead to changes in LpMYO3-mediated phosphorylation of proteins that participate in the photoresponse and thus modify the photoresponse. This idea is consistent with observations showing that the photoresponse is abnormal in *Drosophila* expressing a NINAC that lacks the kinase domain even though the photoreceptors are structurally stable (*11*). The endogenous substrates of LpMYO3, other than LpMYO3 itself, are not

yet known, but previously we showed that the C-terminus of opsin is a candidate (*19*).

In summary, the studies described here present definitive evidence for circadian clock-driven phosphorylation of two sites within the myosin domain of LpMYO3 in LE photoreceptors *in vivo*. One site is within and the other is near loop 2. The identification of these sites permits further investigations into the impact of these phosphorylation events on the function of LpMYO3.

ACKNOWLEDGMENT

We thank Alfred Chung of the UF ICBR Proteomics Core Facility for synthesis of phosphopeptide standards for method validation experiments and Lynn Milstead for preparing figures.

SUPPORTING INFORMATION AVAILABLE

Table 1A−D showing sample calculations for a label-free experiment used to determine clock-driven changes in LpMYO3 phosphorylation. Table 2 showing calculations of methodological and biological errors in the determination of clock-driven changes in LpMYO3 phosphorylation using both differential labeling and label-free methods. This material is available free of charge via the Internet at http://pubs.acs.org.

REFERENCES

1. Montell, C., and Rubin, G. M. (1988) The *Drosophila* ninaC locus encodes two photoreceptor cell specific proteins with domains homologous to protein kinases and the myosin heavy chain head, *Cell 52*, 757−772.
2. Battelle, B-A., Andrews, A. W., Calman, B. G., Sellers, J. R., Greenberg, R. M., and Smith, W. C. (1998) A myosin III from *Limulus* eyes is a clock-regulated phosphoprotein, *J. Neurosci. 18*, 4548−4559.
3. De Velasco, B., Martinez, J. M., Ochoa, G. H., Miller, M. A., Clark, Y. M., Matsumoto, B., and Robles, J. L. (1999) Identification and immunolocalization of actin cytoskeletal components in light- and dark-adapted octopus retinas, *Exp. Eye Res. 68*, 725−737.
4. Dosé, A. C., and Burnside, B. (2000) Cloning and chromosomal localization of a human class III myosin, *Genomics 67*, 333−342.
5. Dosé, A. C., and Burnside, B. (2002) A class III myosin expressed in the retina is a potential candidate for Bardet-Biedl syndrome, *Genomics 79*, 621−624.
6. Dosé, A. C., Hillman, D. W., Wong, C., Sohlberg, L., Lin-Jones, J., and Burnside, B. (2003) Myo3A, one of two class III myosin genes expressed in vertebrate retina, is localized to the calycal processes of rod and cone photoreceptors and is expressed in the sacculus, *Mol. Biol. Cell 14*, 1058−1073.
7. Dosé, A.C., Lin-Jones, J., and Burnside, B. (2004) In *Photoreceptor Cell Biology and Inherited Retinal Degenerations* (Williams, D. S., Ed) pp 133−162.
8. Dalal, J. S., Dosé, A. C., Burnside, B., and Battelle, B-A. (2005) Developmental expression of myo3b in mouse retina, *Invest. Ophthalmol. Vis. Sci. S46*, eAbstract 3964.
9. Walsh, T., Walsh, V., Vreugde, S., Hertzano, R., Shahin, H., Haika, S., Lee, M. K., Kanaan, M., King, M., and Avraham, K. B. (2002) From flies' eyes to our ears: mutations in a human class III myosin cause progressive nonsyndromic hearing loss DFNB30, *Proc. Natl. Acad. Sci. U.S.A. 99*, 7518−7523.
10. Schneider, M. E., Dosé, A. C., Salles, F. T., Chang, W., Erickson, F. L., Burnside, B., and Kachar, B. (2006) A new compartment at stereocilia tips defined by spatial and temporal patterns of myosin IIIa expression, *J. Neurosci. 26*, 10243−10252.
11. Porter, J. A., and Montell, C. (1993) Distinct roles of the *Drosophila ninaC* kinase and myosin domains revealed by systematic mutagenesis, *J. Cell Biol. 1993*, 601−612.
12. Porter, J. A., Yu, M., Doberstein, S. K., Pollard, T. D., and Montell, C. (1993) Dependence of calmodulin localization in the retina on the NINAC unconventional myosin, *Science 262*, 1038−1042.
13. Hofstee, C. A., Henderson, S., Hardie, R. C., and Stavenga, D. G. (1996) Differential effects of NINAC proteins (p132 and p174) on light-activated currents and pupil mechanism in *Drosophila* photoreceptors, *Vis. Neurosci.* 897−906.
14. Chyb, S., Hevers, W., Forte, M., Wolfgang, W. J., Selinger, Z., and Hardie, R. C. (1999) Modulation of the light response by cAMP in *Drosophila* photoreceptors, *J. Neurosci. 19*, 8799−8807.
15. Li, H. S., Porter, J. A., and Montell, C. (1998) Requirement for the NINAC kinase/myosin for stable termination of the visual cascade, *J. Neurosci. 18*, 9601−96067.
16. Ng, K. P., Kambara, T., Matsuura, M., Burke, M., and Ikebe, M. (1996) Identification of myosin III as a protein kinase, *Biochemistry 35*, 9392−9399.
17. Komaba, S., Inoue, A., Maruta, S., Hosoya, H., and Ikebe, M. (2003) Determination of human myosin III as a motor protein having a protein kinase activity, *J. Biol. Chem. 278*, 21352−21360.
18. Dosé, A. C., Ananthanarayanan, S., Moore, J. E., Burnside, M. B., and Yengo, C. M. (2007) Kinetic mechanism of human myosin IIIA, *J. Biol. Chem. 282*, 216−231.
19. Kempler, K. E., Toth, J., Yamashita, R., Mapel, G., Robinson, K., Cardasis, H., Stevens, S., Sellers, J. R., and Battelle, B-A. (2007) Loop 2 of *Limulus* Myosin III is phosphorylated by protein kinase A and autophosphorylation, *Biochemistry 46*, 4280−4293.
20. Kambara, T., Komaba, S., and Ikebe, M. (2006) Human myosin III is a motor having an extremely high affinity for actin, *J. Biol. Chem. 281*, 37291−37301.
21. Battelle, B. A., Dabdoub, A., Malone, M. A., Andrews, A. W., Cacciatore, C., Calman, B. G., Smith, W. C., and Payne, R. (2001) Immunocytochemical localization of opsin, visual arrestin, myosin III, and calmodulin in *Limulus* lateral eye retinular cells and ventral photoreceptors, *J. Comp. Neurol. 435*, 211−225.
22. Fahrenbach, W. H. (1971) The morphology of the *Limulus* visual system. IV. The lateral optic nerve, *Z. Zellforsch. Mikrosk. Anat, 114*, 532−545.
23. Battelle, B-A., Evans, J. A., and Chamberlain, S. C. (1982) Efferent fibers to *Limulus* eyes synthesize and release octopamine, *Science 216*, 1250−1252.
24. Evans, J. A., Chamberlain, S. C., and Battelle, B-A (1983) Autoradiographic localization of newly synthesized octopamine to retinal efferents in the *Limulus* visual system, *J. Comp. Neurol. 219*, 369−383.
25. Battelle, B-A., and Evans, J. A. (1984) Octopamine release from centrifugal fibers of the *Limulus* visual system, *J. Neurochem. 42*, 71−79.
26. Kaupp, U. B., Malbon, C. C., Battelle, B-A., and Brown, J. E. (1982) Octopamine stimulated rise in cAMP in *Limulus* ventral photoreceptors, *Vision Res. 22*, 1503−1506.
27. Edwards, S. C., and Battelle, B-A. (1987) Octopamine- and cyclic AMP-stimulated phosphorylation of a protein in *Limulus* ventral and lateral eyes, *J. Neurosci. 7*, 2811−2820.
28. Edwards, S. C., Andrews, A. W., Renninger, G. H., Wiebe, E. M., and Battelle, B-A. (1990) Efferent innervation to *Limulus* eyes *in vivo* phosphorylates a 122 kD protein, *Biol. Bull. 178*, 267−278.
29. Battelle, B-A. (2002) Circadian efferent input to *Limulus* eyes: anatomy, circuitry, and impact, *Microsc. Res. Tech. 58*, 345−355.
30. Barlow, R. B., Jr., Chamberlain, S. C., and Levinson, J. Z. (1980) *Limulus* brain modulates the structure and function of the lateral eyes, *Science 210*, 1037−1039.
31. Kaplan, E., and Barlow, R. B., Jr. (1980) Circadian clock in *Limulus* brain increases responses and decreases noise of retinal photoreceptors, *Nature 286*, 393−395.
32. Battelle, B-A., Williams, C. D., Schremser-Berlin, J-L., and Cacciatore, C. (2000) Regulation of arrestin mRNA levels in *Limulus* lateral eyes: Separate and combined influences of circadian efferent input and light, *Vis. Neurosci. 17*, 217−227.
33. Chamberlain, S. C., and Barlow, R. B., Jr. (1979) Light and efferent activity control rhabdom turnover in *Limulus* photoreceptors, *Science 206*, 361−363.
34. Chamberlain, S. C., and Barlow, R. B., Jr. (1984) Transient membrane shedding in *Limulus* photoreceptors: control mechanisms under natural lighting, *J. Neurosci. 4*, 2792−2810.
35. Khadilkar, R. V., Mytinger, J. R., Thomason, L. E., Runyon, S. L., Washicosky, K. J., and Jinks, R. N. (2002) Central regulation of photosensitive membrane turnover in the lateral eye of *Limulus.*

I. Octopamine primes the retina for daily transient rhabdom shedding, *Vis. Neurosci. 19*, 283−297.
36. Runyon, S. L., Washicosky, K. J., Brenneman, R. J., Kelly, J. R., Khadilkar, R. V., Heacock, K. F., McCormick, S. M., Williams, K. E., and Jinks, R. N. (2004) Central regulation of photosensitive membrane turnover in the lateral eye of *Limulus*, II: Octopamine acts via adenylate cyclase/cAMP-dependent protein kinase to prime the retina for transient rhabdom shedding, *Vis. Neurosci. 21*, 749−763.
37. Kier, C. K., and Chamberlain, S. C. (1989) Dual controls of screening pigment movement in photoreceptors of the *Limulus* lateral eye: circadian efferent input and light, *Vis. Neurosci.*, *4*, 237−255.
38. Furch, M., Fujita-Becker, S., Geeves, M. A., Holmes, K. C., and Manstein, D. J. (1999) Role of the salt-bridge between switch-1 and switch-2 of *Dictyostelium* myosin, *J. Mol. Biol. 290*, 797−809.
39. Furch, M., Geeves, M., and Manstein, D. J. (1998) Modulation of actin affinity and actomyosin adenosine triphosphatase by charge changes in the myosin motor domain, *Biochemistry 37*, 6317−6326.
40. Joel, P. B., Sweeney, H. L., and Trybus, K. M. (2003) Addition of lysines to the 50/20 kDa junction of myosin strengthens weak binding to actin without affecting the maximum ATPase activity, *Biochemistry 42*, 9160−9166.
41. Ficarro, S. B., McCleland, M. L., Stukenberg, P. T., Burke, D. J., Ross, M. M., Shabanowitz, J., Hunt, D. F., and White, F. M. (2002) Phosphoproteome analysis by mass spectrometry and its application to *Saccharomyces cerevisiae*, *Nat. Biotechnol. 20*, 301−305.
42. Bondarenko, P. V., Chelius, D., and Shaler, T. A. (2002) Identification and relative quantitation of protein mixtures by enzymatic digestion followed by capillary reversed-phase liquid chromatography-tandem mass spectrometry, *Anal. Chem. 74*, 4741−4749.
43. Sineshchekova, O. O., Cardasis, H. L., Severance, E. G., Smith, W. C., and Battelle, B-A. (2004) Sequential phosphorylation of visual arrestin in intact *Limulus* photoreceptors: identification of a highly light-regulated site, *Vis. Neurosci. 21*, 715−724.
44. Laemmli, U. K. (1970) Cleavage of structural proteins during the assembly of the head of bacteriophage T4, *Nature 227*, 680−685.
45. Lowry, O. H., Rosebrough, N. I., Farra, L., and Randall, R. J. (1951) Protein measurement with the Folin phenol reagent, *J . Biol. Chem. 193*, 265−275.
46. Barlow, R. B., Jr. (1983) Circadian rhythms in the *Limulus* visual system, *J. Neurosci. 3*, 856−870.
47. Pieprzyk, A. R., Weiner, W. W., and Chamberlain, S. C. (2003) Mechanisms controlling the sensitivity of the *Limulus* lateral eye in natural lighting, *J. Comp. Neurol. A. 189*, 643−653.
48. Biemann, K. (1992) Mass spectrometry of peptides and proteins, *Annu. Rev. Biochem. 61*, 977−1010.
49. Pearson, R. B., and Kemp, B. E. (1991) Protein kinase phosphorylation site sequences and consensus specificity motifs: Tabulations, In *Methods in Enzymology 200A* (Hunter, T., and Sefton, B. M., Ed.) pp 62−81, Academic Press, San Diego.
50. Sellers, J. R. (1999) *Myosins*, Oxford University Press, New York.
51. Erickson, F. L., Corsa, A. C., Dosé, A. C., and Burnside, B. (2003) Localization of a class III myosin to filopodia tips in transfected HeLa cells requires an actin binding site in its tail domain, *Mol. Biol. Cell 14*, 4173−4180.
52. Hicks, J. L., and Williams, D. S. (1992) Distribution of the myosin I-like NINAC proteins in the *Drosophila* retina and ultrastructural analysis of mutant phenotypes, *J. Cell Sci. 101*, 247−254.
53. Hicks, J. L., Liu, X., and Williams, D. S. (1996) Role of the NINAC proteins in photoreceptor cell structure: ultrastructure of *nina*C deletion mutants and binding to actin filaments, *Cell Motil. Cytoskel. 35*, 367−379.
54. Sacunas, R. B., Papuga, M. O., Malone, M. A., Pearson, A. C., Jr., Marjanovic, M., Stroope, D. G., Weiner, W. W., Chamberlain, S. C., and Battelle, B-A. (2002**)** Multiple mechanisms of rhabdom shedding in the lateral eye of *Limulus polyphemus*, *J. Comp. Neurol. 449*, 26−42.
55. Edwards, S. C., Wishart, A. C., Wiebe, E. M., and Battelle, B.-A. (1989) Light-regulated proteins in *Limulus* ventral photoreceptor cells, *Vis. Neurosci. 3*, 95−105.
56. Minke, B., Rubinstein, C. T., Sahly, I., Bar-Nachum, S., Timberg, R., and Selinger, Z. (1990) Phorbol ester induces photoreceptor-specific degeneration in a *Drosophila* mutant, *Proc. Natl. Acad. Sci. U.S.A. 87*, 113−117.
57. Smith, D. P., Ranganathan, R., Hardy, R. W., Marx, J., Tsuchida, T., and Zuker, C. S. (1991) Photoreceptor deactivation and retinal degeneration mediated by a photoreceptor-specific protein kinase C, *Science 254*, 1478−1484.
58. Jinks, R. N., White, R. H., and Chamberlain, S. C. (1996) Dawn, diacylglycerol, calcium, and protein kinase C−the retinal wrecking crew. A signal transduction cascade for rhabdom shedding in the *Limulus* eye, *J. Photochem. Photobiol. B. 35*, 45−52.

BI701409F